Friction and leakage analysis of the blocker-type valve designed for a revolving vane expander

IOP Conf. Series: Materials Science and Engineering **604** (2019) 012083 doi:10.1088/1757-899X/604/1/012083

Friction and leakage analysis of the blocker-type valve designed for a revolving vane expander

Ali Naseri*, Stuart Norris and Alison Subiantoro

Department of Mechanical Engineering, Faculty of Engineering, the University of Auckland, Auckland, New Zealand

Email: anas222@aucklanduni.ac.nz

Abstract. Friction and leakage are two known issues that contribute to inefficiencies of rotary vane machines, and the Revolving Vane (RV) mechanism was introduced to reduce them. When used as an expander, a mechanism to determine the timing of the suction process in RV machine is required. In this study, a blocker-type valve is proposed for the suction control, and a simulation is carried out to investigate its friction and leakage characteristics. The valve comprises a stationary blocker that blocks high-pressure working fluid from entering the working chambers during expansion. In order to reduce friction, there should be a clearance between the rotary parts and the stationary blocker, which inevitably causes leakage of the working fluid into the working chambers. The leakage was modelled as a compressible flow through a convergent nozzle followed by a Fanno flow through an adiabatic constant cross-section channel. The results showed that the amount of leakage in the absence of lubricants is almost higher than ideal expander flow rate. However, this leakage demonstrated a positive contribution to the output torque as the results of the cylinder wall shear stress. The results suggested the importance of using lubricants in this valve design.

1. Introduction

Expansion machines are widely used to extract energy in various industries, mostly to produce electrical power. Among the available expansion machine types, volumetric ones, such as the rotary vane expander, are predominant for small-scale applications because of their superior characteristics such as their high-pressure ratios, ability to work with two-phase fluid, low flow rates and lower rotational speeds [1]. However, due to the nature of the machine, friction and leakage are the main contributors to their inefficiencies [2, 3]. Several studies have been carried out at lowering the inefficiencies, and among them, the Revolving Vane (RV) mechanism was introduced by Ooi and Teh [4] to eliminate the main contributors to friction losses in rotary machines. This concept comprises a rotor and cylinder that rotate synchronously with respect to their relative axis of rotations as illustrated in Figure 1(B). Vane side friction is reduced by fixing the vane onto the rotor, vane tip friction is completely eliminated since no contact occurs when it moves in the slot, and end face friction is reduced as a result of alleviated relative velocity between the rotor and the cylinder [5].

The design of the suction valve is critical since it dictates the expansion process in RV expander, which may affect the system efficiency. Solenoid valves are not practical due to issues with response time [6]. The relative movement of both the cylinder and the rotor in this mechanism also makes the implementation of wiring complicated [5]. Hence, a specially designed valve is required. Another option is to use a two-stage expander mechanism like that studied by Yang et al. [7] through which the

first and the second expanders are used for the suction and expansion processes, respectively. However, this requires more components and space. Using a stationary blocking system attached to the main casing is a simple solution for the RV expander, as shown by Subiantoro and Ooi [8] who used Teflon made blockers supported by pin and spring to block the suction port at its specified time.

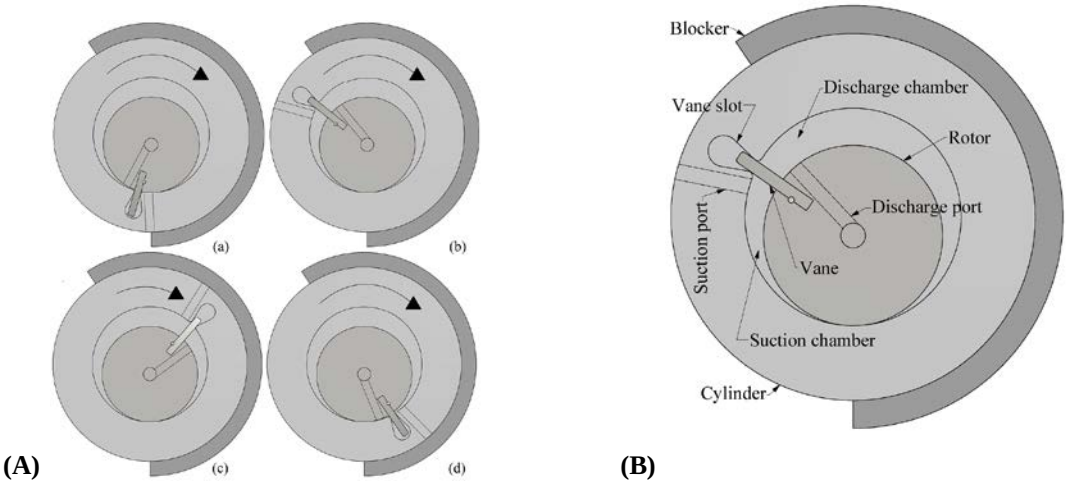

Figure 1. (A) RV Expander operation process, (B) detailed schematic of RV expander.

The valve comprises a stationary blocker that blocks high-pressure working fluid from entering the working chambers during expansion. Figure 1(A) illustrates the process of an RV expander with a stationary blocker. At position (a), suction and discharge processes start and expansion ends. Pressure differences between the suction and discharge chambers and across the vane push the vane and rotor consequently. This increases the fluid mass within the high-pressure suction chamber as well as its volume (position (b)). The expansion process starts when the suction port is covered by the blocker (position (c)) and lasts until it is uncovered, which leads to the discharge process (position (d)). In order to reduce friction between the outer surface of the rotary cylinder and the blocker, there should be a clearance between them. Unfortunately, this inevitably causes leakage of the working fluid into the working chambers. Lubrication can be applied to reduce this leakage. Nevertheless, the blocker's performance has not been studied comprehensively. In this study, the valve's leakage and friction are modelled, and the characteristics and performance of the valve are found.

2. Methodology

2.1. Case study description

The expansion process happens when the suction port is covered by the blocker. Ideally, the mass of fluid in the high-pressure suction chamber is constant as its volume varies. Thus, any leaked flow into this chamber causes deviations from a perfect expansion process.

Figure 2 shows the rubbing surface in the RV mechanism in this study as well as the leakage paths. Although clearance between the outer surface of the rotary cylinder and the stationary blocker minimizes the friction, this causes leakage of working fluid into the working chamber through this gap. Since both ends of the blocker are exposed to the casing-side high-pressure chamber filled with high-pressure working fluid, which will enter the working chamber once the suction port is open, there are two leakage paths into the suction port. Air is considered as the working fluid in this study for simplicity. Following section provides the modelling for the fluid leakage and friction through this clearance gap.

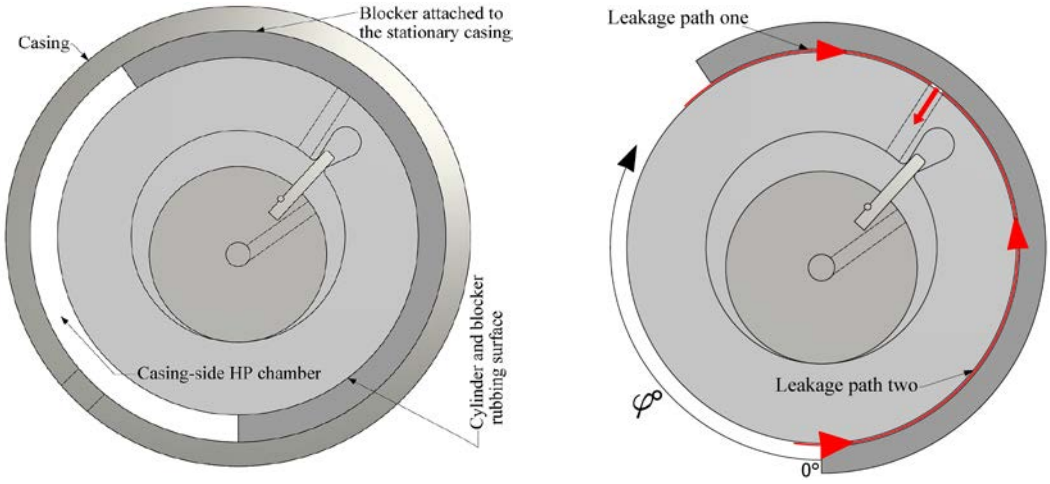

Figure 2. (A) Rubbing surface between rotary and stationary components in RV mechanism, (B) Leakage path with exaggerated thickness.

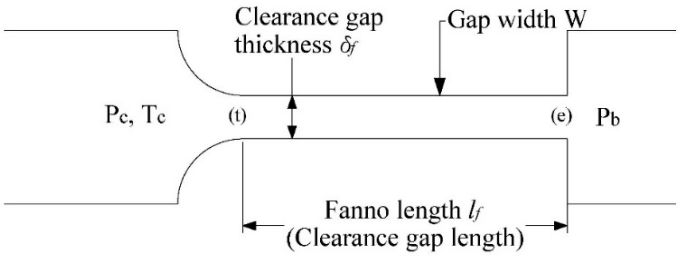

Figure 3. The geometric model for the clearance gap between blocker and cylinder.

2.2. System modelling

Yanagisawa and Shimizu [9] studied the leakage through radial clearance gap in a rolling-piston compressor, which is an important factor affecting the efficiency of volumetric rotary machines, by taking into account of dynamic behaviour and the frictional loss occurring in this narrow channel. They modelled the leakage path with a convergent nozzle followed by a straight channel considering the friction of the walls called Fanno flow [10]. Here, we implemented a similar approach [9] for the compressed air flowing through the clearance gap between the stationary blocker and the rotary cylinder. Figure 3 shows the geometrical model for the clearance gap. In order to model this system, the main dimensions and operating conditions are tabulated in Table 1.

Table 1. Main dimensions and operating conditions.

Expander characteristics [a]			
$R_{cylinder}$ -Cylinder outer radius (mm)	59	Cylinder wall thickness (mm)	24
R_{rotor} - Rotor outer radius (mm)	29	Suction port area (mm^2)	96
δ_f - Gap thickness (μm)	50	$d_h = 2\delta_f$ - Gap hydraulic diameter(mm)	100
W - Gap width (mm)	29	Working chambers maximum volume (cm^3)	30
Operating conditions			
Expander inlet pressure (bar)	6.0	Fluid specific heat ratio	1.4
Expander discharge pressure (bar)	1.0	Suction port closure angle corresponding to the system pressure and maximum volume (°)	145
Expander inlet temperature (K)	298		
Fluid type	Air	Expander rotational speed (rpm)	2500

[a] Refer to [11] for the detailed dimensions.

In order to model the system, Reynolds number (*Re*), and Darcy friction factor (λ) in the clearance gap are calculated according to Equations (1) and (2).

$$\mathrm{Re} = \frac{2Q_m}{\mu W} \tag{1}$$

$$\lambda = 96\,\mathrm{Re}^{-1}\,(if\ \mathrm{Re} \le 3560)\,,\ \ 0.3164\,\mathrm{Re}^{-0.25}\,(if\ \mathrm{Re} > 3560) \tag{2}$$

Where Q_m, W and μ are the mass flow rate through the gap, gap width and thickness, respectively. It is worth mentioning that the laminar-turbulent transition was assumed instantaneous in Equation (2). Assuming Mach number at the outlet of the channel (Ma_e) as unity, Mach number at the throat (Ma_t) corresponding to the specified channel length is obtained using Equation (3).

$$\frac{\overline{\lambda} l_f}{2\delta} = \frac{1-Ma_t}{kMa_t^2} + \frac{k+1}{2k}\ln\left\{\frac{(k+1)Ma_t^2}{2+(k-1)Ma_t^2}\right\} \tag{3}$$

Where $\overline{\lambda} = \lambda$, l_f , δ and k are the average friction factor in the channel, the effective Fanno length for the channel, channel thickness, and the fluid specific heat ratio, respectively. The pressure ratios at the clearance gap and convergent nozzle are given in Equations (4) and (5).

$$\frac{P_t}{P_e} = \frac{1}{Ma_t}\left(\frac{k+1}{2+(k-1)Ma_t^2}\right)^{1/2} \tag{4}$$

$$\frac{P_c}{P_t} = \left(1+\frac{k-1}{2}Ma_t^2\right)^{k/k-1} \tag{5}$$

Where Ma_t is the calculated Mach number at the clearance inlet using Equation (3). Comparing the total pressure ratio $\zeta = P_c.P_e^{-1} = Pc.P_t^{-1} \times P_t.P_e^{-1}$, and the given pressure ratio across the gap $P_c.P_b^{-1}$, fluid is choked only if $P_c.P_e^{-1} < P_c.P_b^{-1}$. Hence, the Mach at the outlet is equal to unity and the fluid temperature, velocity and mass flow rate at the channel outlet can be calculated by Equations (8) to (10). If the fluid is not choked, using assumed Ma_t at the channel inlet, the imaginary critical channel length (l_f^*) at which flow is sonic at the outlet of the channel can be obtained using Equation (3) and the clearance gap and convergent nozzle pressure ratios can be again calculated using Equations (4) and (5). Consequently, Mach number at the channel outlet (Ma_e) can be calculated by solving Equation (6). Using l_f^*, Mach number at the outlet of the channel is calculated by solving Equation (6).

$$\frac{\overline{\lambda}(l_f^* - l_f)}{2\delta} = \frac{1-Ma_e}{kMa_e^2} + \frac{k+1}{2k}\ln\left\{\frac{(k+1)Ma_e^2}{2+(k-1)Ma_e^2}\right\} \tag{6}$$

Where l_f, δ and k are channel length and thickness, and the fluid specific heat ratio, respectively. The critical pressure ratio can be calculated according to Equation (7).

$$\frac{P_e}{P^*} = \frac{1}{Ma_e}\left(\frac{k+1}{2+(k-1)Ma_e^2}\right)^{1/2} \tag{7}$$

Where P^* is the sonic pressure and P_e is the pressure at the channel outlet. The total pressure ratio is then obtained from $P_c.P_e^{-1} = P_c.P_t^{-1} \times P_t\ .P^{*-1} \times P^*.P_e^{-1}$. If $P_c.P_e^{-1} = P_c.P_b^{-1}$, the assumed Ma_t and the calculated Ma_e are valid and fluid properties can be calculated by Equations (8) to (10). Otherwise, a new assumption for Ma_t should be made until it satisfies the condition above.

$$T_e = T_c\left\{1+\frac{(k-1)Ma_e^2}{2}\right\}^{-1} \tag{8}$$

$$V_e = Ma_e \times \left(kR_gT_e\right)^{1/2} \tag{9}$$

$$Q_{m,e} = \delta W P_e V_e \times \left(R_gT_e\right)^{-1} \tag{10}$$

In Equations (9) and (10), V_e and R_g stand for velocity at the channel outlet and the gas constant, respectively.

Figure 4 illustrates the flowchart for mass flow rate calculations. To calculate wall shear stress at the surface of the control volume, Equation (11) is used. Darcy friction factor in this equation is given by Equation (2) [10]. Moreover, the total torque exerted on the cylinder body because of leakage flows at an individual angle can be calculated using Equation (12) in which R stands for the cylinder radius.

$$\tau_w = \frac{1}{8}\rho\lambda V^2 = \frac{1}{8}\lambda kPMa^2 \tag{11}$$

$$\int_{\deg} dT_{loss} = R_{cylinder} \times \int_{wall} \tau_w dA \tag{12}$$

To solve Equation (12), the leakage path length at every studied angle is discretized into *160* nodes, corresponding to a maximum discretization uncertainty of 1.97%, which is equal to $2.8\times10^{-4}\ N.m/\deg$ (refer to [12] for the detailed calculations). It is noteworthy that the Couette flow effect on the friction factor and wall shear stress was neglected for the simplicity, and considering the fact that the tangential velocity of the cylinder at the walls was far less compared to the fluid speed in the channel.

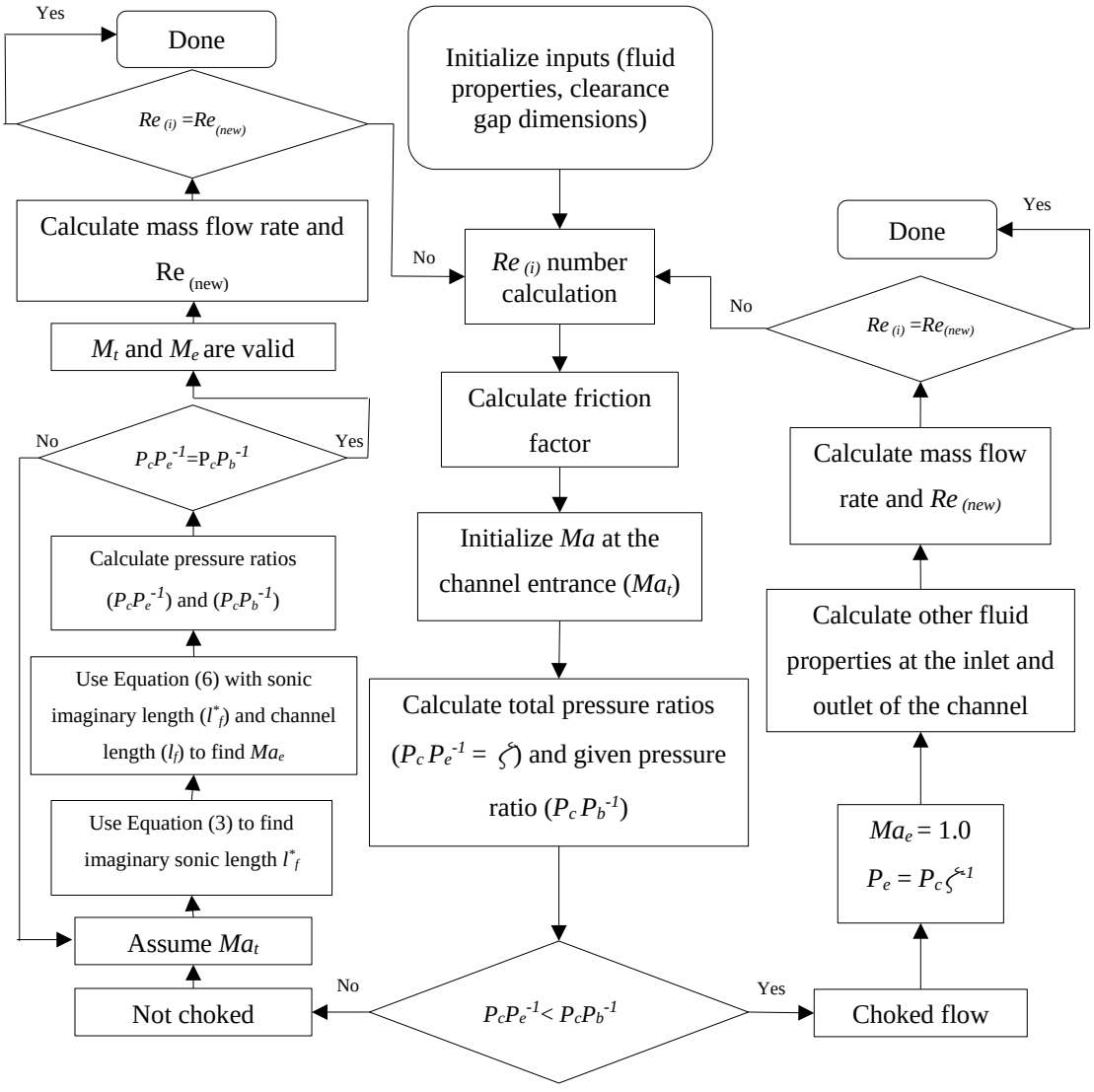

Figure 4. Flowchart of leakage flow rate calculation in the model.

3. Model validation

In order to validate the model described in section 2.2, a comparison with results from the air leakage modelling for two gap thicknesses of a previous study [9] was carried out. This was achieved assuming the main dimensions and operating conditions provided by the reference study, and for two different gap thicknesses, 23 and 46 µm. The results presented in Figure 5 shows a small 3.6% average error between simulation results from the reference and this study, which are comparable to the reference results. It is noteworthy that the fluid properties in this study were obtained using CoolProp [13] at each step of the simulation shown in Figure 4.

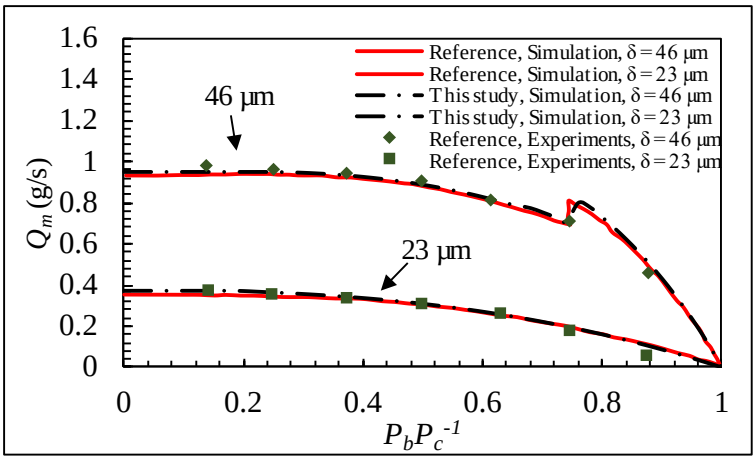

Figure 5. Validation results for the air leakage with P_c = 0.79 MPa, T_c = 300 K [9].

4. Results

In this study, a perfect isentropic expansion process was assumed in the expander. Hence, the suction port should be covered by the blocker from an angle corresponding to the start of the isentropic expansion process, which was calculated by the maximum and minimum pressures of the expander and their corresponding chamber volumes. Since the position of suction port changes with rotation of the cylinder, the lengths of leakage paths change too. Moreover, the pressure differences across the leakage paths vary as the result of expansion taking place in the chamber.

Figure 6(A) illustrates the pressure alteration inside the working chamber. As the expander rotated and the suction port was covered by the blocker, which was the start of the expansion, the pressure difference across the leakage paths increased. Furthermore, Figure 6(B) illustrates changes in the length of leakage paths at the specified operation conditions in Table 1. It can be seen that the length of path one increased while path two shortened, leading to different behaviors of leakage through the two gaps.

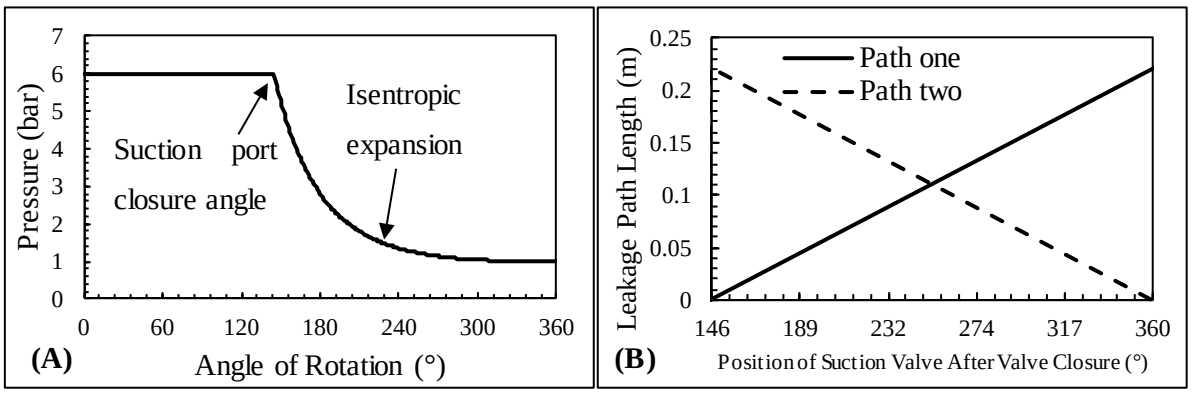

Figure 6. (A) Leakage paths length, (B) Pressure alteration in the suction chamber.

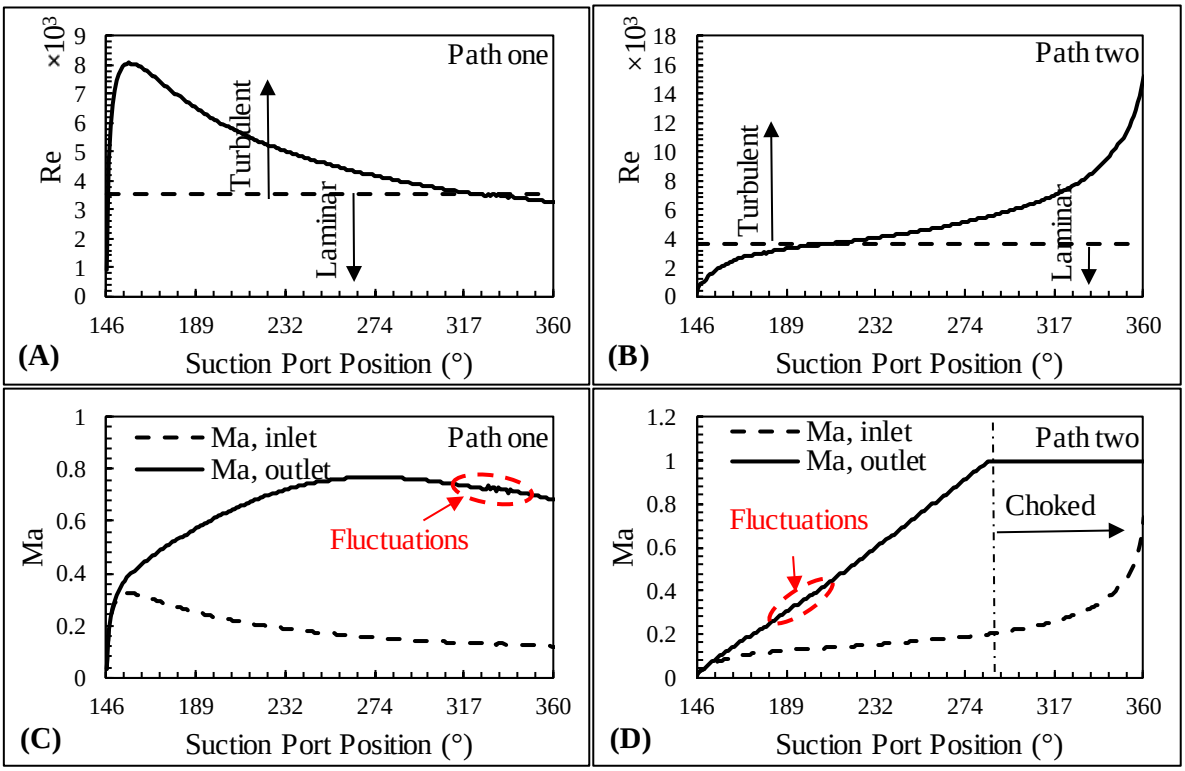

Figure 7. Re and Ma numbers variation versus position of suction port.

Figure 7 compares the Reynold number variation for the leakage as well as changes in Mach number for both paths for their inlet and outlet. Since the laminar-turbulent transition was assumed instantaneous, there was a small-amplitude fluctuation, as shown in Figure 7(C) and (D), corresponding to the angles at which the fluid regime changed from turbulent to laminar and vice versa.

As the suction port moved, at the very first angles of the blocking process, a sudden small pressure drop occurred across both paths due to the exponential nature of the isentropic process. Meanwhile, there was only a small change in the length of the path. Since the length of path one was already small, a remarkable increase in fluid velocity was witnessed that changed fluid regime to turbulent at that very first angles. Consequently, *Re* and *Ma* numbers rose as shown in Figure 7(A) and (C). For path two, this growth occurred in much smaller amplitudes since this path was longer than path one. Hence, the fluid regime changed to turbulent in the later angles. The trends of these growths are shown in Figure 7(B) and (D). Nevertheless, as the pressure drop was small, the dimensionless speed at the inlet and outlet had roughly the same trends for both paths. Hereafter, the exponential increment in pressure drop across the leakage paths as well as a linear increase and decrease in the lengths of path one and two, respectively, led to a separation in the inlet and outlet *Ma* numbers shown in Figure 7(C) and (D).

For path one, as the pressure drop went to a plateau and the length increased, fluid velocity decreased and the fluid underwent a laminar regime, Figure 7(A). This also caused a drop in the *Ma* number as shown in Figure 7(C).

For path two, since both length and the changes in pressure difference decreased, a considerable growth occurred in the flow speed. This led to choking at the path outlet from a specific angle onwards as shown in Figure 7(D). Further decrease in length at a roughly plateaued pressure difference led to an increase at the inlet speed to approach a sonic condition at the outlet of the path two (see Figure 7(B)). Therefore, *Ma* increased rapidly as the length approached the minimum (Figure 7(D)).

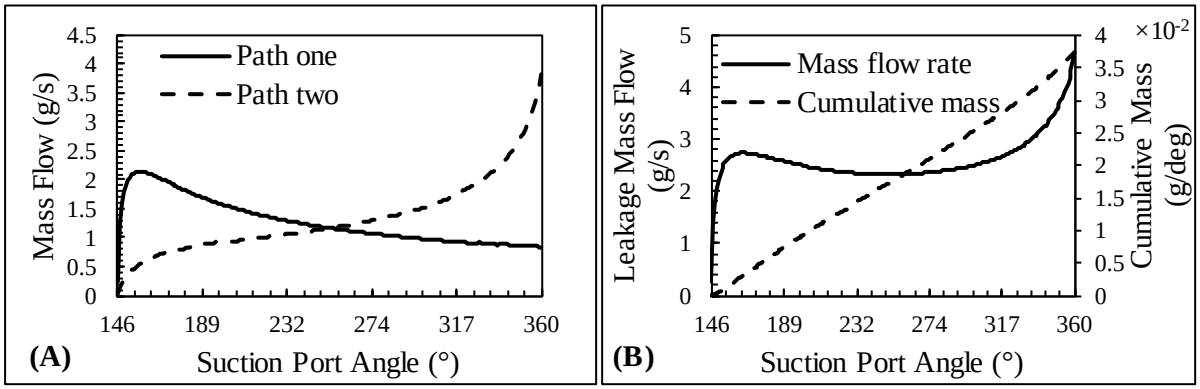

Figure 8. (A) Total leaked flow rate versus suction port angle as well as cumulative leaked mass (B) Leakage mass flow rate versus suction port angle for both paths.

Figure 8(A) presents the total leakage at individual angles. Having calculated the *Re* number, the leakage flow rate was obtained from Equation (1). Hence, the trend of the leakage flow rate for both paths was the same as what is shown in Figure 7(A) and (B). It should be noted that the mass flow rate was calculated for individual angles per each revolution of the expander. Figure 8(B) presents the total leaked mass flow rate as the summation of leakage in both paths. There should be 35 mg of air in the suction chamber during a perfect isentropic expansion at each rotation of expander. This was calculated using the equations derived for an adiabatic and isentropic revolving vane mechanism with no frictional and leakage losses in reference [11] assuming the main dimensions and operating conditions provided in Table 1. Meanwhile, the cumulative mass result showed that about 37.5 mg of fluid leaked to the suction port at each rotation of expander. This is approximately the same as the mass of air in the expander, indicating a very severe leakage if no lubrication is applied.

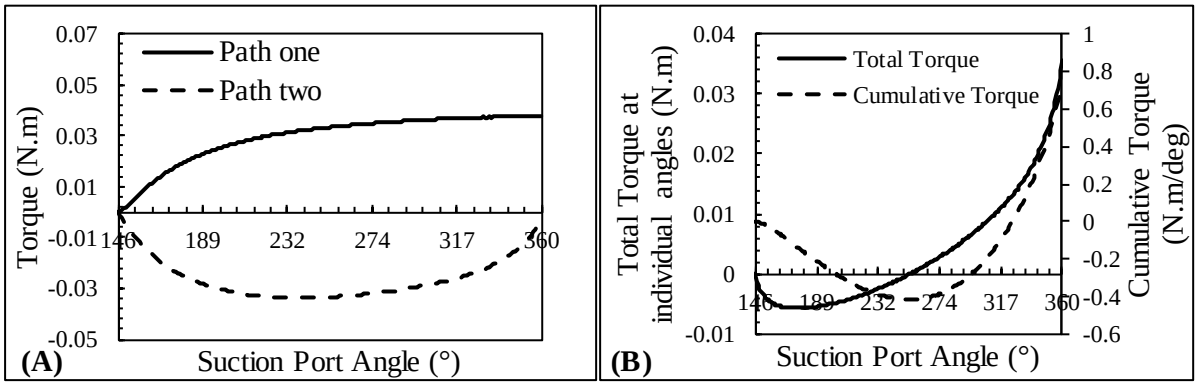

Figure 9. Torque exerts on the cylinder in the rotational direction of the expander.

Figure 9(A) illustrates how friction torque exerted by the leakage on the cylinder varied in the expander's rotational direction for both paths. As shown in Figure 9(A), the frictional torque of the leakage flow in path one was always in the rotational direction of the expander. This added an extra torque to the expander output and increased the mechanical efficiency. However, path two reduced the expander output torque. To interpret the trend of the total torque output, the product of pressure and square of *Ma* number in Equation (11) was used. According to Figure 6(B), pressure was descending at the outlet of leakage paths. This product reached its maximum after a sudden increase, for the leakage through path one. This mainly occurred as the result of rapid growth in *Ma* number (Figure 7(C)). However, the product increased more smoothly afterward since the pressure drop became approximately constant, and the *Ma* number reduced. As the suction port continued to move, the friction area increased. Eventually, the product of area and shear stress on the wall ($\tau_w dA$) increased.

As for path two, the product of pressure and square of *Ma* number was always growing since the fluid was speeding up to reach a sonic outlet while the friction area decreased. Therefore, after an increase in torque on the opposite direction of rotation, the decreasing friction area overweighed the effect of increasing *Ma* number. Hence, the product of area and shear stress on the wall ($\tau_w dA$) decreased after reaching a peak in the opposite direction of the expander rotation (see Figure 9(A)).

Figure 9(B) shows the summation of torque exerted on the cylinder due to the leakage in both paths. The leakage decreased the torque output when the suction port went up to 253° while it escalated the output torque once it passed the angle above. However, the total positive contribution of leakage to the output torque was 0.745 N·m at each revolution, while the system produces 0.37 N·m per revolution calculated by the dynamic and static parameters for the system. This was again calculated using the equations derived for an adiabatic and isentropic revolving vane mechanism with no frictional and leakage losses in reference [11] assuming the main dimensions and operating conditions provided in Table 1. This is almost double that of ideal output torque for the expander. The torque caused by the leakage was very high because it was calculated using the outer radius and area of the cylinder, which were almost double that of radius and area for the chambers. Therefore, the torque was significant although the force due to wall shear stress was not. Moreover, the cumulative torque meaning the summation of torque at desired angle and all the angles before is presented in this figure. This shows the alteration of total torque output at different angles over a revolution.

Comparing the result of leaked mass and output torque shows the importance of using lubricants in this valve design. The results showed that the amount of leaked flow in the absence of lubricant is about the same as the required one for the perfect expansion process. It is worthy to mention that in practice, the leakage may interrupt the expansion of fluid and increases pressure at the expansion chamber over the expansion process, and over-expansion happens. This on the one hand increases the area under the pressure-volume diagram leading to higher ideal output torque for the expander, and on the other hand, decreases leaked flow to the chambers. However, in this study it was assumed that the pressure inside the chamber follows isentropic process during the expansion and the effect of pressure changes inside the chambers was ignored.

5. Conclusions

Friction and leakage are two known issues contributing to inefficiencies of rotary vane machines, and the Revolving Vane (RV) mechanism was introduced to reduce such inefficiencies. In this study, a blocker-type valve was proposed for the suction control in a Revolving Vane expander. A simulation was carried out to investigate the leakage and friction characteristics of this valve. In order to reduce friction between the outer surface of the rotary cylinder and the blocker, there should be a clearance in between the two surfaces. Unfortunately, this inevitably causes leakage of the working fluid into the working chambers. The leakage through this gap was modelled as a compressible flow through a convergent nozzle followed by a Fanno flow through an adiabatic constant cross-section channel in this study. The results showed that for a gap of 50 μm the amount of leaked flow in the absence of lubricant was about 37.5 mg per revolution, while the ideal expander flow rate was about 35 mg in each revolution. Furthermore, the total positive contribution of leakage to the output torque was 0.745 N·m at each revolution, while the system produces 0.37 N·m per revolution. The results suggested the importance of using lubricants in this valve design. In this study, it was assumed that the pressure inside the chamber follows isentropic process during the expansion and the effect of pressure changes inside the chambers was ignored. Further study needs to be carried out in the future to find the actual leakage and friction values with the presence of lubricant.

Nomenclatures

A	Area (*m*)	*Greek*	
k	Specific heat ratios	δ_f	Clearance gap thickness(μm)
l_f	Fanno length (*mm*)	λ	Friction factor

Ma	Mach number	μ	Kinematic viscosity (*Pa.s*)
P	Pressure (*bar*)	ρ	Density (kg/m^3)
Q_m	Mass flow rate (*kg/s*)	τ	Wall shear stress (*Pa*)
Re	Reynolds number	ζ	Pressure ratio
R_g	Gas constant (*J/kgK*)	*Subscript*	
R	Cylinder/rotor radius (*mm*)	b	Suction chamber
T	Temperature (*K*), Torque (*N.m*)	c	Casing side high pressure chamber
V	Velocity (*m/s*)	e	Clearance gap/channel outlet
W	Gap width (*mm*)	t	Clearance gap/channel inlet

References

[1] Lemort, V., Quoilin, S., Cuevas, C., and Lebrun, J. (2009). Testing and modeling a scroll expander integrated into an Organic Rankine Cycle. *Applied Thermal Engineering*, ***29***(14-15), 3094-3102.

[2] Badr, O., O'Callaghan, P. W., Hussein, M., and Probert, S. D. (1984). Multi-vane expanders as prime movers for low-grade energy organic Rankine-cycle engines. *Applied Energy*, ***16***(2), 129-146.

[3] Mohd.Tahir, M. , Yamada, N. , Hoshino, T. (2010). Efficiency of Compact Organic Rankine Cycle System with Rotary-Vane-Type Expander for Low-Temperature Waste Heat Recovery. *World Academy of Science, Engineering and Technology, International Science Index 37, International Journal of Mechanical, Aerospace, Industrial, Mechatronic and Manufacturing Engineering*, **4**(1), 105 – 110.

[4] Ooi, K. T., and Teh, Y. L. (2012). *U.S. Patent No. 8,206,140*. Washington, DC: U.S. Patent and Trademark Office.

[5] Subiantoro, A., and Ooi, K. T. (2009). Introduction of the revolving vane expander. *HVAC&R Research*, ***15***(4), 801-816.

[6] Baek, J. S., Groll, E. A., and Lawless, P. B. (2005). Piston-cylinder work producing expansion device in a transcritical carbon dioxide cycle. Part I: Experimental investigation. *International Journal of Refrigeration*, ***28***(2), 141-151.

[7] Yang, J., Zhang, L., and Shi, Y. J. (2006). Development and performance analysis of a two cylinder rolling piston expander for transcritical CO_2 system. *International Compressor Engineering Conference.*

[8] Subiantoro, A., and Ooi, K. T. (2012). Analysis of the revolving vane (RV-0) expander, Part 1: Experimental investigations. *International Journal of Refrigeration*, ***35***(6), 1734-1743.

[9] Yanagisawa, T., and Shimizu, T. (1985). Leakage losses with a rolling piston type rotary compressor. I. Radical clearance on the rolling piston. *International Journal of Refrigeration*, ***8***(2), 75-84.

[10] White, F.M., *Fluid Mechanics*, *WCB.* Ed McGraw-Hill Boston, 1999.

[11] Subiantoro, A. (2012). Development of a revolving vane expander (Doctoral dissertation). Nanyang Technological University, Singapore.

[12] Celik, I. B. (2007). Procedure for estimation and reporting of discretization error in CFD applications. *Journal of Fluids Engineering editorial policy statement on the control of numerical accuracy.*

[13] Bell, I. H., Wronski, J., Quoilin, S., and Lemort, V. (2014). Pure and pseudo-pure fluid thermophysical property evaluation and the open-source thermophysical property library CoolProp. *Industrial and engineering chemistry research*, **53**(6), 2498-2508.